Title: Functional assessment of sodium chloride cotransporter NCC mutants in polarized mammalian epithelial cells.

Authors: Rosenbaek LL, Rizzo F, MacAulay N, Staub O, Fenton RA

Journal: American journal of physiology. Renal physiology

Year: 2017 Aug 1

Issue: 313

Volume: 2

Pages: F495-F504

DOI: 10.1152/ajprenal.00088.2017

Functional Assessment of Sodium Chloride Co-transporter NCC Mutants in Polarized Mammalian Epithelial Cells

Lena L Rosenbaek[1,2], Federica Rizzo[3,4], Nanna MacAulay[2], Olivier Staub[3,4] and Robert A. Fenton[1]

[1]InterPrET Center, Department of Biomedicine, Aarhus University, Aarhus DK-8000, Denmark, [2]Department of Neuroscience and Pharmacology, University of Copenhagen, Copenhagen, Denmark, [3]Department of Pharmacology & Toxicology, University of Lausanne, Lausanne, Switzerland, [4]National Centre of Competence in Research "Kidney.ch", Switzerland

Running title: NCC uptake assay in polarized mammalian cells

Keywords: *Slc12a3*, thiazide-sensitive co-transporter, cotransporter, phosphorylation, sodium flux assay

Correspondence:
Robert A. Fenton
Aarhus University
Institute for Biomedicine
Wilhelm Meyers Allé 3, Building. 1233
DK- 8000 Aarhus C
Denmark
Tel: +0045 87167671
E-mail: robert.a.fenton@biomed.au.dk

Abstract

The thiazide-sensitive sodium chloride cotransporter, NCC, is important for maintaining serum sodium (Na^+) and, indirectly, serum potassium (K^+) levels. Functional studies on NCC have used cell lines with native NCC expression, transiently transfected non-polarized cell lines or *Xenopus laevis* oocytes. Here, we developed the use of polarized Madin-Darby canine kidney type I (MDCKI) mammalian epithelial cell lines with tetracycline-inducible human NCC expression to study NCC activity and membrane abundance in the same system. In radiotracer assays, induced cells grown on filters had robust thiazide-sensitive and chloride dependent sodium-22 (^{22}Na) uptake from the apical side. To minimize cost and maximize throughput, assays were modified to use cells grown on plastic. On plastic, cells had similar thiazide-sensitive ^{22}Na uptakes that increased following pre-incubation of cells in chloride-free solutions. NCC was detected in the plasma membrane and both membrane abundance and phosphorylation of NCC were increased by incubation in chloride-free solutions. Furthermore, in cells exposed for 15 min to low or high extracellular K^+, the levels of phosphorylated NCC increased and decreased, respectively. To demonstrate that the system allows rapid and systematic assessment of mutated NCC, three phosphorylation sites in NCC were mutated and NCC activity examined. ^{22}Na fluxes in phosphorylation deficient mutants were reduced to baseline levels, whereas phosphorylation mimicking mutants were constitutively active – even without chloride-free stimulation. In conclusion, this system allows the activity, cellular localization, and abundance of wildtype or mutant NCC to be examined in the same polarized mammalian expression system in a rapid, easy, and low cost fashion.

Introduction

The kidney plays a key role in blood pressure control by modulating the levels of NaCl reabsorption. Although the majority of NaCl reabsorption occurs in the proximal tubules, the distal convoluted tubules (DCT) play an essential role in the fine-tuning of tubular fluid NaCl concentrations. DCT NaCl transport is tightly regulated by a variety of hormones e.g. vasopressin (8, 29) and angiotensin II (35, 42), which exert the majority of their effects by modulating the function of the sodium chloride cotransporter NCC, the predominant NaCl entry pathway in this segment (reviewed in (10)). NCC is a member of the SLC12 electroneutral cation-coupled chloride cotransporter family, which also includes the sodium potassium chloride cotransporters, NKCC1 and NKCC2, as well as several potassium chloride cotransporters (KCCs). Inactivating mutations of NCC lead to the autosomal recessive kidney disorder Gitelman syndrome, characterized by hypokalemia, hypomagnesemia, metabolic alkalosis, and hypocalciuria (22, 24, 27, 36). In Gordon's syndrome (PHAII or familial hyperkalemic hypertension), increased activity of NCC is observed, resulting in hyperkalemic hypertension (15).

In the last few years, a large number of studies performed using *Xenopus laevis* oocytes (14, 28, 34, 43) or mammalian cell lines expressing native NCC (5, 13, 19-21, 32), have advanced our understanding on how alterations in NCC localization or NCC activity interplay to determine the final rate of NaCl reabsorption (reviewed in (26)). For example, 1) the activity of NCC is regulated by posttranslational modifications such as phosphorylation, ubiquitylation, and glycosylation (11, 17); 2) NCC is functional in a highly glycosylated homodimeric form (6, 12, 17, 31); 3) phosphorylation of NCC is critical for maximal NaCl transport capacity (15) and can alter NCC membrane abundance (33); 4) phosphorylation of NCC is regulated by a variety of hormonal stimuli, which exert several of their effects via

activation of the WNK-SPAK kinase cascade (15) Despite these major advances, a limitation in the field has been the lack of a suitable system that allows a direct comparison of NCC activity and localization in a polarized mammalian cell system alongside the capacity to examine wildtype NCC or various forms of NCC carrying targeted mutations e.g. specific post-translational modification or Gitelman's causing mutations. Therefore, the aim of this study was to develop a ^{22}Na uptake assay for direct assessment of the function of wildtype or mutant NCC in a polarized mammalian cell line. The assays are based on Type I MDCK (Madin-Darby Canine Kidney) cells containing FRT (flippase recognition target) sites with tetracycline-inducible NCC expression (33). We demonstrate that these cells can be rapidly modified to express various forms of NCC from a single genomic site, allowing direct comparison of the abundance, activity, and localization of wildtype and mutant NCC in a single system.

Materials and Methods

Antibodies – The antibodies used in this study are rabbit polyclonal antibodies against total NCC (a kind gift from Dr. Mark Knepper, NIH, Bethesda, Maryland, USA)(18), phosphorylated NCC (pT58) (29) and FLAG-tag (F7425, Sigma).

Generation of tetracycline inducible NCC expressing MDCKI cell lines - A FLAG-tag (GACTACAAGGACGATGACGATAAG; amino acids DYKDDDDK) was introduced into the NH2-terminus of a human NCC (hNCC) cDNA using standard methods. Using PCR, the FLAG-tagged hNCC sequence was subcloned into the pcDNA5/FRT/TO/TOPO vector (Invitrogen). The pcDNA5/FRT/TO/TOPO-hNCC plasmid was cotransfected with pOG44 (encoding flp recombinase) into tetracycline inducible MDCK type I cells line containing a single FRT site in their genome (33) using Lipofectamine 2000 (Invitrogen). Cells with stable insertion of the hNCC into the FRT site were selected using 500 μg/ml Hygromycin B. Stable MDCKI-hNCC cell lines were maintained in DMEM High Glucose with 10% DBS, 150 μg/ml Hygromycin B, and 5 μg/ml Blasticidin HCl. Generation of the various MDCKI-rNCC cell lines have been described previously (33).

Quantitative reverse transcriptase PCR (RT-qPCR) and standard RT-PCR - RNA was purified using the RiboPureTM kit (Ambion) following the manufacturer's protocol. Potential DNA contamination was removed by incubating RNA (500ng) with DNase I Amp Grade 1 in DNase Reaction buffer (20 mM Tris-HCl, pH 8.4, 2 mM $MgCl_2$, 50 mM KCl) (Invitrogen) for 15 min at room temperature. 1.1 mM EDTA was added, and the samples were heated to 65 °C for 10 min to stop the DNase reaction. cDNA was produced following the protocol from SuperScriptTM II reverse transcriptase (Invitrogen). Subsequently, 250 ng cDNA and 10

pmole gene specific primer were used for qPCR using LightCycler® 480 SYBR Green I Master (Roche). The reaction was carried out by a LightCycler® 480 (Roche) using NCC specific primers (forward: 5'TCCTCAAGCAGGAAGGTAGC3', reverse: 5'GTTCTCCAGGGCTCTTCTCG3'). Primers against 18SrRNA were used for normalization (forward: 5'GGATCCATTGGAGGGCAAGT3', reverse: 5'ACGAGCTTTTTAACTGCAGCAA3'). For standard RT-PCR, cDNA was generated in a similar manner from MDCK cells or dog kidney RNA (Zyagen) and PCR performed using HotStarTaq (Qiagen), 250 ng cDNA and 10 pmole gene specific primers and standard conditions. Primers used were: *Slc12a2* (forward: 5'-GCCCTGCTGTCCCCTTAAAT, reverse: 5'-CGTGCAACTGGGAGACTCAT), *Slc12a1* (forward: 5'-GCTGAACATCTGGGGTGTCA-, reverse: 5'-CCTTTTGTGAAGCTTGGCCC), *Slc26a4* (forward: 5'-CGATCCATAGCCTCGTGCTT, reverse: 5'-CCGGTGGGTAAATCTTGCCT), *Slc4a8* (forward: 5'-GACTACCGGGATGCACTCAG-, reverse: 5'-ATTGGCCCACTGGACTTCTG), *Scnn1a* (forward: 5'-CGAAGTCCCTGTGGAGAACC, reverse: 5'-CTCCGCATTCTTGGGCAATG), *Slc9a1* (forward: 5'-CGAGGACATCTGTGGCCATT, reverse: 5'-GATAACAGGCAAGTCGGCCT), *Slc9a3* (forward: 5'-GCGAACATCACTCAAGACGC, reverse: 5'-GATCCTGACATCTCAGCGGG), *Kcnj10* (forward: 5'-CCTCTTCTCCCTCGAATCGC, reverse: 5'-TGTCGACCTGGAAAGTCACG).

Sample preparation and immunoblotting – Cells were washed in PBS-CM (PBS, 1 mM $CaCl_2$, 0.1 mM $MgCl_2$, pH 7.5), solubilized in 1x Laemmli sample buffer (62.5 mM Tris base pH 6.8, 8.7% glycerol, 2% SDS, 1% bromphenolblue, 100 mM dithiothreitol) and heated for 15 min at 60 °C. SDS-PAGE was performed on 4-15% gradient polyacrylamide gels

(Criterion TGX Precast Protein Gels, BioRad) and transferred to PVDF membrane. Antibody-antigen reactions were visualized using SuperSignal West Femto chemiluminescent substrate (Thermo Scientific, Denmark). Semi-quantitative data were obtained by analysis of band densities using Image Studio Lite (Qiagen) and relative abundance ratios for each individual sample for each time point or stimulant were calculated. All reported values are means ± S.E.M.

Cell surface biotinylation assay - Cells were grown in complete DMEM (DMEM High Glucose, 10% DBS) to confluency. Cells were induced with 10 μg/ml tetracycline for 16-20 hours prior to biotinylation. Cells were washed twice in isotonic buffer (135 mM NaCl, 5 mM KCl, 1 mM $CaCl_2$, 1 mM $MgCl_2$, 1 mM Na_2HPO_4, 1 mM Na_2SO_4, 15 mM Na^+ HEPES, pH 7.4) and stimulated with either low chloride buffer (67.5 mM Na^+ gluconate, 2.5 mM K^+ gluconate, 0.5 mM $CaCl_2$, 0.5 mM $MgCl_2$, 1 mM Na_2HPO_4, 1 mM Na_2SO_4, 7.5 mM Na^+ HEPES, pH 7.4) or isotonic buffer and incubated for 20 min at 37 °C. Cells were washed in ice-cold PBS-CM and incubated with mild agitation for 30 min at 4 °C in ice-cold biotinylation buffer (10 mM triethanolamine, 2 mM $CaCl_2$, 125 mM NaCl, pH 8.9) containing a 1 mg/ml final concentration of sulfosuccinimidyl 2-(biotin-amido)-ethyl-1,3-dithiopropionate (EZ-link Sulfo-NHS-SS-biotin, Pierce). Cells were washed in ice-cold quenching buffer (PBS-CM, 50 mM Tris-HCl, pH 8) followed by two washes of PBS-CM. Cells were lysed and biotinylated proteins purified using NeutrAvidin gel slurry (Pierce) as previously described (33).

Immunoprecipitation (IP) - Performed as previously described (33).

Extracellular K^+ manipulation - Cells were grown in complete DMEM (DMEM High Glucose, 10% DBS) to confluency and induced with 10 μg/ml tetracycline for 16-20 hours prior to experiment. Cells were washed twice in Ringer solution (98.5 mM NaCl, 3 mM KCl, 2.5 mM $CaCl_2$, 1.8 mM $MgCl_2$, 1 mM NaH_2PO_4, 25 mM $NaHCO_3$, 25 mM glucose) and incubated for 15 min at 37 °C in either Ringer solution, Ringer solution containing 1mM KCl, Ringer solution containing 6mM KCl, or low chloride buffer. An equimolar adjustment of NaCl ensured that osmolality of the solutions remained constant between the different [K^+] (100.5mM NaCl or 95.5 mM NaCl). Cells were solubilized in 1x Laemmli sample buffer.

^{22}Na uptake assay to measure NCC activity - Cells were grown in complete DMEM to confluency and induced for 16-20 hours with 10 μg/ml tetracycline. Subsequently, cells were washed in pre-heated (37°C) serum free DMEM medium and incubated (where indicated) for 20 min at 37°C in chloride-free buffer (130 mM Na gluconate, 2 mM K gluconate, 1 mM Ca gluconate, 1 mM Mg gluconate, 5 mM HEPES, and 5 mM Tris-HCl, pH 7.4) including 1 mM Ouabain, 1 mM amiloride, 0.1 mM benzamil, and 0.1 mM bumetanide, with 0.1 mM Metolazone (where indicated). Metolazone dose response experiments were performed with concentrations ranging from 10^{-3} to 10^{-8} M. Cells were subsequently incubated in uptake buffer (140 mM NaCl, 1 mM $CaCl_2$, 1 mM $MgCl_2$, 5 mM HEPES, and 5 mM Tris pH 7.4 including inhibitors) with 1.5 μCi/ml ^{22}NaCl for 20 min at 37°C. For the chloride dependency experiment, uptake was performed in either normal uptake buffer or a chloride free uptake buffer (140 mM Na gluconate, 2 mM K gluconate, 1 mM Ca gluconate, 1 mM Mg gluconate, 5 mM HEPES, and 5 mM Tris-HCl, pH 7.4). Cells were rapidly and extensively washed in ice cold uptake buffer without radioisotope and lysed in 500 µl of PBS with 0.1% SDS. The average counts in the last wash from 3 samples was collected to determine background

activity, which was subsequently subtracted from all cell-specific radioactive measurements. All radioactivity measurements were performed in a Cobra II 5002 Auto-Gamma counter (Packard) with a counting efficiency of approximately 95%. 20 µl of each lysed sample was used to determine total protein concentration using the BCA Protein Assay Kit (Pierce).

Statistical analysis - One-way analyses of variance or Tukey's multiple comparisons tests were performed as appropriate using Graphpad Prism. Experimental numbers (n) are reported in individual figures. Values are considered statistically significant when $p < 0.05$.

Results

Generation and characterization of an MDCKI cell line with tetracycline inducible human NCC expression.

A schematic overview of the procedure for generating MDCK type I stable cell lines expressing tetracycline inducible human NCC (or another gene of interest (GOI)) is shown in Fig 1A. Several cell lines were generated and characterized based on cell morphology, NCC expression levels, and NCC trafficking to the apical plasma membrane. One individual clone (termed MDCKI-hNCC) was used for the remainder of this study. Immunoprecipitation of hNCC using a FLAG-tag antibody followed by western blotting against NCC identified hNCC as a non-glycosylated band of approximately 100 kDa, a mature glycosylated smeared band ~130 kDa, and as dimeric forms above 250 kDa (**Fig 1B**). No hNCC was detected in similar cells in the absence of tetracycline. To assess if the expression of hNCC correlated with increased NaCl transport into MDCKI cells, ^{22}Na uptake assays were developed. In MDCKI-hNCC cells grown on semi-permeable supports there was a significantly higher ^{22}Na uptake following treatment with tetracycline relative to non-treated controls (**Fig 1C**). Following incubation of tetracycline treated MDCKI-hNCC cells with metolazone (a thiazide that inhibits NCC activity), ^{22}Na uptake was decreased. A small decrease in ^{22}Na uptake was also observed in non-induced MDCKI-hNCC cells with metolazone, indicating either a small leakiness in NCC expression, or the presence of a minor alternative metolazone-sensitive NaCl entry pathway in MDCKI cells. To examine the latter possibility, the expression of other Na^+ transport proteins in our MDCKI-hNCC cells was examined by RT-PCR (**Fig 2**). The sodium potassium chloride cotransporter 1 (NKCC1), the Na^+-driven $Cl^-/HCO3^-$ exchanger (NDCBE), the alpha-subunit of the epithelial sodium channel (ENaC) and the sodium hydrogen exchanger 1 (NHE1) were detected in

our MDCKI cells, whereas NKCC2, Pendrin and the sodium hydrogen exchanger 3 (NHE3) were absent. As NDCBE is inhibited by thiazide (23, 37), it is a good candidate for the minor alternative metolazone-sensitive NaCl entry pathway in MDCKI-hNCC cells.

Comparison of MDCKI-hNCC cells grown on plastic or semi-permeable supports.

Due to the high cost of growing cells in large numbers on semi-permeable supports, and the technical difficulty in handling numerous separate filters rapidly at the same time, we wanted to transfer the uptake assay to cells grown on plastic support. Visually, MDCKI-hNCC cells grown on plastic plates formed a tight confluent monolayer of hexagonal shaped cells (**Fig 3A**). Immunoprecipitation of hNCC using a FLAG-tag antibody from cells grown on plastic support followed by western blotting identified hNCC as a non-glycosylated band of around 100 kDa and a smear of approximately 130 kDa (**Fig 3B**), corresponding to the immature non-glycosylated and mature glycosylated monomeric form of NCC, respectively. The dimeric form of NCC was not consistently observed in MDCKI-hNCC cells grown on plastic plates. No NCC was detected in non-induced cells. As previously observed (**Fig 1**), tetracycline-induced MDCKI-hNCC cells grown on semi-permeable supports had a significantly higher metolazone sensitive ^{22}Na uptake relative to non-treated controls (**Fig 3C**). Metolazone sensitive ^{22}Na uptake was also observed in MDCKI-hNCC cells grown on plastic. However, the magnitude of ^{22}Na uptake in plastic grown cells relative to semi-permeable supports was significantly less (**Fig 3C)**. The reduced uptake in plastic grown cells relative to semi-permeable support grown cells corresponded with significantly less hNCC (**Fig. 3D and E**). As metolazone sensitive ^{22}Na uptake could consistently be measured in MDCKI-hNCC cells grown on plastic, the remainder of studies were performed on this support.

Characterization of ^{22}Na uptake in MDCKI-hNCC cells grown on plastic supports

To further assess the characteristics of ^{22}Na uptake in plastic grown MDCKI-hNCC cells, the effects of uptake time, metolazone dose, and chloride dependency were determined. Incubation of tetracycline-induced cells in uptake solution for various times demonstrated increased ^{22}Na uptake as a function of time, with apparent time-linearity up to 40 min (r^2 = 0.95, no significant deviation from linearity) (**Fig 4A**). To ensure all uptakes were performed within the linear range, we continued to perform subsequent uptakes with a 20 min incubation time. Metolazone inhibition experiments allowed generation of a dose-response curve of ^{22}Na uptake (**Fig. 4B**). The calculated IC50 for metolazone was 0.43 x 10^{-6}M, with maximal inhibition of ^{22}Na uptake occurring between 3-10 μM. The degree of ^{22}Na uptake in MDCKI-hNCC cells incubated in uptake medium without chloride ions (chloride-free buffer, CF) was comparable to levels after metolazone inhibition, demonstrating chloride dependency of the ^{22}Na uptake and indicating a requirement for NCC in the transport process (**Fig. 4C**).

Chloride-free pre-incubation of MDCKI-hNCC cells increases Na^+ *uptake*

We have previously shown that incubation of semi-permeable support grown MDCKI cells expressing rat NCC in low chloride medium increases apical plasma membrane abundance of NCC and phosphorylation of NCC at an activating site (pT58-NCC). These events are associated with decreased rates of NCC internalization (33). Similar results are observed for plastic grown MDCKI-hNCC cells, with the levels of biotinylated total NCC and pT58-NCC being significantly greater following incubation in low chloride solution (**Fig 5A-C**). Correspondingly, ^{22}Na uptakes were significantly higher in MDCKI-hNCC cells pre-

incubated in CF medium relative to chloride-containing (CC) medium (**Fig 5D**), indicating that in these cells a combination of increased NCC membrane expression and NCC phosphorylation correlates with greater ^{22}Na uptakes.

Acute changes in extracellular K^+ concentration modulates pT58-NCC levels in MDCKI-hNCC cells.

The activity of NCC can be directly modulated by extracellular [K^+] (39), a process that is dependent on alterations in membrane voltage and activity of the potassium channel Kir4.1 (3). To assess if similar changes in NCC were evident in our system, MDCKI-hNCC cells were incubated for 15 min in buffers with different [K^+](as KCl) and pT58-NCC levels assessed by immunoblotting (**Fig 6A**). pT58-NCC levels were inversely correlated with the extracellular [K^+] (**Fig 6B**). These changes occurred despite an absence of Kir4.1 in MDCKI-hNCC cells (**Fig 2**), suggesting an alternative K^+ channel is involved in the response. Furthermore, low extracellular [K^+] increased pT58-NCC levels significantly more than incubation of cells in low chloride buffer, emphasizing that both Cl^--dependent and -independent WNK-SPAK signalling pathways are modulated by extracellular [K+] (30).

Preventing phosphorylation of NCC decreases Na^+ uptake, while phosphorylation-mimicking mutants of NCC are constitutively active

To emphasize the advantages of our MDCKI isogenic stable cell lines for characterization of various NCC mutants, we performed uptake studies in MDCKI cell lines expressing; 1) rat NCC (rNCC); 2) “phospho-deficient” NCC mutants where Thr-53, Thr-58, and Ser-71 are converted to alanine (TTS-AAA) or; 3) “phospho-mimicking” NCC mutants where Thr-53, Thr-58, and Ser-71 are converted to aspartic acid (TTS-DDD) (33). Immunoprecipitation of

297 rNCC using a FLAG-tag antibody followed by western blotting identified rNCC as a non-
298 glycosylated band of approximately 100 kDa, a mature glycosylated smeared band ~130
299 kDa, and as dimeric forms above 250 kDa (**Fig 7A**). No NCC was detected in the absence
300 of tetracycline. Following tetracycline induction, apical surface biotinylation followed by
301 immunoprecipitation demonstrated similar NCC protein levels in the 3 different cell lines (**Fig**
302 **7B**), which correlated with no significant differences in rNCC mRNA expression between the
303 lines (**Fig 7C**). As observed for MDCKI-hNCC cells (**Fig 5A**), MDCKI-rNCC cells grown on
304 plastic had significantly higher metolazone sensitive ^{22}Na uptakes following pre-incubation
305 CF relative to CC medium (**Fig 7D)**. Under CF pre-incubation conditions, metolazone-
306 sensitive ^{22}Na uptakes in MDCKI-rNCC TTS-AAA cells were significantly lower than in
307 MDCKI-rNCC cell lines, and almost undetectable when chloride was present in the pre-
308 incubation medium. In contrast, ^{22}Na uptakes in MDCKI-rNCC TTS-DDD mutants were
309 significantly higher than MDCKI-rNCC cells and independent of the presence of chloride in
310 the pre-incubation medium (**Fig 7D**).
311
312

Discussion

Although some studies have utilized mammalian cell lines to assess NCC function and activity, the systems used suffer from some disadvantages (summary in Table 1); 1) some have endogenous NCC expression and are thus unsuitable for assessing the activity of various NCC mutants (13, 19-21); 2) some cell lines used are not polarized and thus regulated delivery of NCC to the cell surface may be different from native cells (32); 3) the cells express NCC transiently and therefore suffer from differences in gene copy number and mRNA expression making comparisons between mutants difficult (5, 32, 40). Therefore, the majority of functional assessments of NCC, comprising a wealth of data, arise from the use of the *Xenopus laevis* expression system (4, 14, 28, 34, 43). Although this system possesses some excellent features that make it a good model system (reviewed in (25)), there exist a number of disadvantages that limit its usefulness in studying NCC function. These disadvantages include the potential for temperature-sensitive processes such as protein trafficking or transporter activity to be altered in the oocyte (derived from a poikilothermic animal), the possibility that polarized trafficking of NCC and accessory proteins are different, and the concern that complex signaling cascades and signaling specificities within oocytes are different from mammalian systems e.g. contradictory role of WNK kinases for modulation of NCC (reviewed in (1, 15)). Thus, the aim of the present study was to develop a single system that allowed for direct comparison between NCC or different NCC mutants in respect to their activity or polarized trafficking events and which had intact mammalian intracellular signaling networks.

The system developed utilizes MDCKI cells, which are highly characterized for studying polarized membrane protein trafficking (9, 16, 33). The cells have a single FRT site (33) and were modified to allow tetracycline-inducible expression of NCC or NCC mutants

337 from a single genetic locus ((33). The advantage of this approach is that the copy number,
338 rate/degree of transcription, and the subsequent mRNA expression of each NCC form (as
339 long as mRNA degradation is unaltered) should be similar (see Fig 7), and differences in
340 NCC abundance can be attributed to post-transcriptional effects. Also, these MDCKI cells
341 possess several elements of the signaling pathways that regulate NCC, e.g. the protein
342 kinases SPAK, OSR1, and WNK1, -3, -4 (33), making them a suitable *in vitro* system for
343 assessment of NCC regulatory events. This was emphasized in the current study (Fig 6),
344 where the levels of phosphorylated NCC following alterations in extracellular [K^+] mimicked
345 the *in vivo* situation (30, 39). In the MDCKI cells, as we previously observed for rat NCC
346 (33), human NCC existed as a highly glycosylated protein with the capacity to form dimers
347 (Fig 1). This is an important attribute of the MDCKI-hNCC cells relative to other NCC
348 expression systems where NCC exists predominantly as a high-mannose glycoprotein (19,
349 21, 38), as NCC is functional as a homodimer and complex glycosylation is a prerequisite
350 for the functional expression of NCC on the apical plasma membrane (4, 6, 17).

351 MDCKI-hNCC cells displayed robust thiazide-sensitive ^{22}Na uptake when cultured on
352 semi-permeable supports or plastic (Fig 3). Despite reduced NCC expression, the thiazide-
353 sensitive Na^+ uptakes in MDCKI-hNCC cells cultured on plastic were routinely higher than
354 controls. The reasons for different NCC expression between the supports are unknown, but
355 they may result from reduced polarization of the MDCK cells on plastic or the inability to
356 absorb/secrete substances across the basolateral plasma membrane. Despite this, NCC
357 was readily detected in the surface biotinylated pool of these cells (Fig 5) and uptake time
358 frames (20 min), chloride dependency, and metolazone concentrations for maximal uptake
359 inhibition were comparable to previous ^{22}Na uptake studies in mammalian cell models (7,
360 21). Combined with the easier handling, potential for higher sample numbers, and the lower

experimental costs, culturing MDCKI-hNCC cells on plastic for assessment of NCC activity was deemed to be optimal.

Studies in oocytes or mammalian cells have demonstrated that NCC phosphorylation, plasma membrane abundance, and activity can be increased by intracellular chloride depletion (28, 32, 33). Here we demonstrated that, following intracellular chloride depletion, similar alterations in NCC function are detectable in MDCKI-hNCC cells grown on plastic. If necessary, we are able to measure NCC activity without prior intracellular chloride depletion (Fig 5), allowing us to examine regulated NCC activity, for example due to hormones such as vasopressin or angiotensin II, without prior maximal stimulation of the regulatory SPAK/OSR1 pathway. Using such an approach allowed us to demonstrate, for the first time in mammalian cells, that by mimicking NCC phosphorylation at Thr53, Thr58, and Ser71 (rat nomenclature, MDCKI-rNCC TTS-DDD mutant cells), NCC is constitutively active, whereas eliminating phosphorylation at these sites (TTS-AAA rNCC mutants) reduced ^{22}Na uptake to baseline values. These data further support the idea that these sites in NCC are critical for NCC function (2, 32, 41).

In summary, our polarized MDCKI cell model allows rapid and direct assessment of the function of different NCC mutants. The cells can be utilized to examine the activity, localization, and abundance of different NCC mutants in the same system, and as such is highly complementary to other models currently being utilized.

Acknowledgements.

We would like to thank Helle Høyer, Tina Drejer, Ahmed Abduljabar, and Christian Westberg for technical assistance. Ole Bækgaard Nielsen, Department of Biomedicine, Aarhus University is thanked for help with radiotracer studies. The original non-inducible MDCKI-FRT cells were kindly provided by Dr. Otto Froehlich, Emory University, USA (deceased).

Grants.

Funding for this study (to RAF) was provided by the Novo Nordisk Foundation, the Lundbeck Foundation and the Danish Medical Research Council. Further funding (to OS) was provided by the Swiss National Science Foundation Grant # 310030_159735, the National Centre of Competence in Research “Swiss Kidney.ch”, networking support by the COST Action ADMIRE BM1301, the Novartis Foundation for medical-biological research. LLR is supported by the Danish Medical Research Council (Ref. DFF – 4092-00128).

Disclosures

No conflicts of interest, financial or otherwise, are declared by the authors.

Author contributions

LLR: performed experiments, analyzed data, and wrote first draft of manuscript. FR: performed experiments. NM: assisted in conception and design of experiments and analyzed data. OS: assisted in conception of experiments and analyzed data. RAF: performed experiments, conception and design of experiments, data analysis, edited and finalized manuscript. All authors approved the final version of manuscript.

References

1. **Bazua-Valenti S, and Gamba G**. Revisiting the NaCl cotransporter regulation by with-no-lysine kinases. *Am J Physiol Cell Physiol* 308: C779-791, 2015.
2. **Chiga M, Rai T, Yang SS, Ohta A, Takizawa T, Sasaki S, and Uchida S**. Dietary salt regulates the phosphorylation of OSR1/SPAK kinases and the sodium chloride cotransporter through aldosterone. *Kidney international* 74: 1403-1409, 2008.
3. **Cuevas CA, Su XT, Wang MX, Terker AS, Lin DH, McCormick JA, Yang CL, Ellison DH, and Wang WH**. Potassium Sensing by Renal Distal Tubules Requires Kir4.1. *Journal of the American Society of Nephrology : JASN* 2017.
4. **De Jong JC, Van Der Vliet WA, Van Den Heuvel LP, Willems PH, Knoers NV, and Bindels RJ**. Functional expression of mutations in the human NaCl cotransporter: evidence for impaired routing mechanisms in Gitelman's syndrome. *Journal of the American Society of Nephrology : JASN* 13: 1442-1448, 2002.
5. **de Jong JC, Willems PH, Goossens M, Vandewalle A, van den Heuvel LP, Knoers NV, and Bindels RJ**. Effects of chemical chaperones on partially retarded NaCl cotransporter mutants associated with Gitelman's syndrome in a mouse cortical collecting duct cell line. *Nephrology, dialysis, transplantation : official publication of the European Dialysis and Transplant Association - European Renal Association* 19: 1069-1076, 2004.
6. **de Jong JC, Willems PH, Mooren FJ, van den Heuvel LP, Knoers NV, and Bindels RJ**. The structural unit of the thiazide-sensitive NaCl cotransporter is a homodimer. *The Journal of biological chemistry* 278: 24302-24307, 2003.
7. **de Jong JC, Willems PH, van den Heuvel LP, Knoers NV, and Bindels RJ**. Functional expression of the human thiazide-sensitive NaCl cotransporter in Madin-

Darby canine kidney cells. *Journal of the American Society of Nephrology : JASN* 14: 2428-2435, 2003.

8. **Elalouf JM, Roinel N, and de Rouffignac C**. Effects of antidiuretic hormone on electrolyte reabsorption and secretion in distal tubules of rat kidney. *Pflugers Archiv : European journal of physiology* 401: 167-173, 1984.

9. **Frohlich O, Klein JD, Smith PM, Sands JM, and Gunn RB**. Urea transport in MDCK cells that are stably transfected with UT-A1. *Am J Physiol Cell Physiol* 286: C1264-1270, 2004.

10. **Gamba G**. Molecular physiology and pathophysiology of electroneutral cation-chloride cotransporters. *Physiological reviews* 85: 423-493, 2005.

11. **Gamba G**. Regulation of the renal Na+-Cl- cotransporter by phosphorylation and ubiquitylation. *American journal of physiology Renal physiology* 303: F1573-1583, 2012.

12. **Gamba G, Miyanoshita A, Lombardi M, Lytton J, Lee WS, Hediger MA, and Hebert SC**. Molecular cloning, primary structure, and characterization of two members of the mammalian electroneutral sodium-(potassium)-chloride cotransporter family expressed in kidney. *The Journal of biological chemistry* 269: 17713-17722, 1994.

13. **Gesek FA, and Friedman PA**. Sodium entry mechanisms in distal convoluted tubule cells. *The American journal of physiology* 268: F89-98, 1995.

14. **Glover M, Mercier Zuber A, Figg N, and O'Shaughnessy KM**. The activity of the thiazide-sensitive Na(+)-Cl(-) cotransporter is regulated by protein phosphatase PP4. *Canadian journal of physiology and pharmacology* 88: 986-995, 2010.

15. **Hadchouel J, Ellison DH, and Gamba G**. Regulation of Renal Electrolyte Transport by WNK and SPAK-OSR1 Kinases. *Annu Rev Physiol* 78: 367-389, 2016.

16. **Hoffert JD, Fenton RA, Moeller HB, Simons B, Tchapyjnikov D, McDill BW, Yu MJ, Pisitkun T, Chen F, and Knepper MA**. Vasopressin-stimulated increase in phosphorylation at Ser269 potentiates plasma membrane retention of aquaporin-2. *The Journal of biological chemistry* 283: 24617-24627, 2008.

17. **Hoover RS, Poch E, Monroy A, Vazquez N, Nishio T, Gamba G, and Hebert SC**. N-Glycosylation at two sites critically alters thiazide binding and activity of the rat thiazide-sensitive Na(+):Cl(-) cotransporter. *Journal of the American Society of Nephrology : JASN* 14: 271-282, 2003.

18. **Kim GH, Masilamani S, Turner R, Mitchell C, Wade JB, and Knepper MA**. The thiazide-sensitive Na-Cl cotransporter is an aldosterone-induced protein. *Proceedings of the National Academy of Sciences of the United States of America* 95: 14552-14557, 1998.

19. **Ko B, Joshi LM, Cooke LL, Vazquez N, Musch MW, Hebert SC, Gamba G, and Hoover RS**. Phorbol ester stimulation of RasGRP1 regulates the sodium-chloride cotransporter by a PKC-independent pathway. *Proceedings of the National Academy of Sciences of the United States of America* 104: 20120-20125, 2007.

20. **Ko B, Kamsteeg EJ, Cooke LL, Moddes LN, Deen PM, and Hoover RS**. RasGRP1 stimulation enhances ubiquitination and endocytosis of the sodium-chloride cotransporter. *American journal of physiology Renal physiology* 299: F300-309, 2010.

21. **Ko B, Mistry AC, Hanson L, Mallick R, Cooke LL, Hack BK, Cunningham P, and Hoover RS**. A new model of the distal convoluted tubule. *American journal of physiology Renal physiology* 303: F700-710, 2012.

22. **Lemmink HH, Knoers NV, Karolyi L, van Dijk H, Niaudet P, Antignac C, Guay-Woodford LM, Goodyer PR, Carel JC, Hermes A, Seyberth HW, Monnens LA, and van den Heuvel LP**. Novel mutations in the thiazide-sensitive NaCl cotransporter gene in patients with Gitelman syndrome with predominant localization to the C-terminal domain. *Kidney international* 54: 720-730, 1998.

23. **Leviel F, Hubner CA, Houillier P, Morla L, El Moghrabi S, Brideau G, Hassan H, Parker MD, Kurth I, Kougioumtzes A, Sinning A, Pech V, Riemondy KA, Miller RL, Hummler E, Shull GE, Aronson PS, Doucet A, Wall SM, Chambrey R, and Eladari D**. The Na+-dependent chloride-bicarbonate exchanger SLC4A8 mediates an electroneutral Na+ reabsorption process in the renal cortical collecting ducts of mice. *J Clin Invest* 120: 1627-1635, 2010.

24. **Mastroianni N, Bettinelli A, Bianchetti M, Colussi G, De Fusco M, Sereni F, Ballabio A, and Casari G**. Novel molecular variants of the Na-Cl cotransporter gene are responsible for Gitelman syndrome. *American journal of human genetics* 59: 1019-1026, 1996.

25. **Moeller HB, and Fenton RA**. Can one Bad Egg' really spoil the batch? *J Physiol* 588: 2283-2284, 2010.

26. **Moes AD, van der Lubbe N, Zietse R, Loffing J, and Hoorn EJ**. The sodium chloride cotransporter SLC12A3: new roles in sodium, potassium, and blood pressure regulation. *Pflugers Archiv : European journal of physiology* 466: 107-118, 2014.

27. **Monkawa T, Kurihara I, Kobayashi K, Hayashi M, and Saruta T**. Novel mutations in thiazide-sensitive Na-Cl cotransporter gene of patients with Gitelman's syndrome. *Journal of the American Society of Nephrology : JASN* 11: 65-70, 2000.

28. **Pacheco-Alvarez D, Cristobal PS, Meade P, Moreno E, Vazquez N, Munoz E, Diaz A, Juarez ME, Gimenez I, and Gamba G**. The Na+:Cl- cotransporter is activated and phosphorylated at the amino-terminal domain upon intracellular chloride depletion. *The Journal of biological chemistry* 281: 28755-28763, 2006.

29. **Pedersen NB, Hofmeister MV, Rosenbaek LL, Nielsen J, and Fenton RA**. Vasopressin induces phosphorylation of the thiazide-sensitive sodium chloride cotransporter in the distal convoluted tubule. *Kidney international* 78: 160-169, 2010.

30. **Penton D, Czogalla J, Wengi A, Himmerkus N, Loffing-Cueni D, Carrel M, Rajaram RD, Staub O, Bleich M, Schweda F, and Loffing J**. Extracellular K+ rapidly controls NaCl cotransporter phosphorylation in the native distal convoluted tubule by Cl- -dependent and independent mechanisms. *J Physiol* 594: 6319-6331, 2016.

31. **Plotkin MD, Kaplan MR, Verlander JW, Lee WS, Brown D, Poch E, Gullans SR, and Hebert SC**. Localization of the thiazide sensitive Na-Cl cotransporter, rTSC1 in the rat kidney. *Kidney international* 50: 174-183, 1996.

32. **Richardson C, Rafiqi FH, Karlsson HK, Moleleki N, Vandewalle A, Campbell DG, Morrice NA, and Alessi DR**. Activation of the thiazide-sensitive Na+-Cl- cotransporter by the WNK-regulated kinases SPAK and OSR1. *Journal of cell science* 121: 675-684, 2008.

33. **Rosenbaek LL, Kortenoeven ML, Aroankins TS, and Fenton RA**. Phosphorylation Decreases Ubiquitylation of the Thiazide-sensitive Co-transporter NCC and

Subsequent Clathrin-mediated Endocytosis. *The Journal of biological chemistry* 2014.

34. **San-Cristobal P, Pacheco-Alvarez D, Richardson C, Ring AM, Vazquez N, Rafiqi FH, Chari D, Kahle KT, Leng Q, Bobadilla NA, Hebert SC, Alessi DR, Lifton RP, and Gamba G**. Angiotensin II signaling increases activity of the renal Na-Cl cotransporter through a WNK4-SPAK-dependent pathway. *Proceedings of the National Academy of Sciences of the United States of America* 106: 4384-4389, 2009.

35. **Sandberg MB, Riquier AD, Pihakaski-Maunsbach K, McDonough AA, and Maunsbach AB**. ANG II provokes acute trafficking of distal tubule Na+-Cl(-) cotransporter to apical membrane. *American journal of physiology Renal physiology* 293: F662-669, 2007.

36. **Simon DB, Nelson-Williams C, Bia MJ, Ellison D, Karet FE, Molina AM, Vaara I, Iwata F, Cushner HM, Koolen M, Gainza FJ, Gitleman HJ, and Lifton RP**. Gitelman's variant of Bartter's syndrome, inherited hypokalaemic alkalosis, is caused by mutations in the thiazide-sensitive Na-Cl cotransporter. *Nature genetics* 12: 24-30, 1996.

37. **Sinning A, Radionov N, Trepiccione F, Lopez-Cayuqueo KI, Jayat M, Baron S, Corniere N, Alexander RT, Hadchouel J, Eladari D, Hubner CA, and Chambrey R**. Double Knockout of the Na+-Driven Cl-/HCO3- Exchanger and Na+/Cl- Cotransporter Induces Hypokalemia and Volume Depletion. *Journal of the American Society of Nephrology : JASN* 28: 130-139, 2017.

543 38. **Subramanya AR, Liu J, Ellison DH, Wade JB, and Welling PA**. WNK4 diverts the
544 thiazide-sensitive NaCl cotransporter to the lysosome and stimulates AP-3
545 interaction. *The Journal of biological chemistry* 284: 18471-18480, 2009.
546 39. **Terker AS, Zhang C, McCormick JA, Lazelle RA, Zhang C, Meermeier NP, Siler**
547 **DA, Park HJ, Fu Y, Cohen DM, Weinstein AM, Wang WH, Yang CL, and Ellison**
548 **DH**. Potassium modulates electrolyte balance and blood pressure through effects on
549 distal cell voltage and chloride. *Cell Metab* 21: 39-50, 2015.
550 40. **Valdez-Flores MA, Vargas-Poussou R, Verkaart S, Tutakhel OA, Valdez-Ortiz A,**
551 **Blanchard A, Treard C, Hoenderop JG, Bindels RJ, and Jelen S**. Functionomics
552 of Ncc Mutations in Gitelman Syndrome Using a Novel Mammalian Cell-Based
553 Activity Assay. *American journal of physiology Renal physiology* ajprenal 00124
554 02016, 2016.
555 41. **Vallon V, Schroth J, Lang F, Kuhl D, and Uchida S**. Expression and
556 phosphorylation of the Na+-Cl- cotransporter NCC in vivo is regulated by dietary salt,
557 potassium, and SGK1. *American journal of physiology Renal physiology* 297: F704-
558 712, 2009.
559 42. **van der Lubbe N, Lim CH, Fenton RA, Meima ME, Jan Danser AH, Zietse R, and**
560 **Hoorn EJ**. Angiotensin II induces phosphorylation of the thiazide-sensitive sodium
561 chloride cotransporter independent of aldosterone. *Kidney international* 79: 66-76,
562 2011.
563 43. **Wilson FH, Kahle KT, Sabath E, Lalioti MD, Rapson AK, Hoover RS, Hebert SC,**
564 **Gamba G, and Lifton RP**. Molecular pathogenesis of inherited hypertension with
565 hyperkalemia: the Na-Cl cotransporter is inhibited by wild-type but not mutant WNK4.

Proceedings of the National Academy of Sciences of the United States of America 100: 680-684, 2003.

569 ***Figure legends***

570

571 **Fig 1: Characterization of an MDCKI cell line with tetracycline inducible human NCC**
572 **expression. A:** The host MDCKI cell line contains a single FRT site and a zeocin resistance
573 gene integrated into its genome and expresses a tetracycline repressor (TR). Co-
574 transfection of pcDNA5/FRT/TO/TOPO-hNCC and pOG44 (encoding flp recombinase) into
575 the host cell line triggers homologous recombination at the FRT sites, resulting in cells with
576 a single copy of the NCC gene integrated into a specific site and displaying hygromycin
577 resistance. NCC expression is controlled by tetracycline induction via two TR binding sites
578 upstream of the NCC gene. Tetracycline treatment releases the 2xTR and transcription of
579 NCC occurs. **B:** NCC immunoprecipitated from MDCKI-hNCC cells grown on semi-
580 permeable supports using a rabbit FLAG-tag antibody. NCC is detected as a non-
581 glycosylated band of approximately 100 kDa, a glycosylated band around 130 kDa, and a
582 higher molecular weight protein above 250 kDa (possible glycosylated NCC dimers). **C:**
583 Quantitative assessment of ^{22}Na uptake in MDCKI-hNCC cells grown on semi-permeable
584 supports. Cells were treated where indicated with tetracycline for 16-20 hours before uptake.
585 Uptake was performed in uptake medium +/- metolazone as indicated. ^{22}Na uptake was
586 increased by tetracycline induction and inhibited by metolazone. Data are means ± S.E.M.
587 (*n*=6). *Represents significant differences compared to tetracycline induced cells without
588 metolazone inhibition. **Represents significant differences compared to non-induced cells
589 without metolazone inhibition

590

591 **Fig 2: RT-PCR analysis of various other transport proteins in MDCKI-hNCC cells**
592 **grown on semi-permeable supports.**

Fig 3: Comparison of MDCKI-hNCC cells cultured on semi-permeable supports or plastic. A: MDCKI-hNCC cells grown on plastic form a confluent monolayer of hexagonal shaped cells. **B:** NCC immunoprecipitated using a rabbit FLAG-tag antibody from MDCKI-hNCC cells grown on plastic. NCC is detected as a band around 100 kDa and a smear of approximately 130 kDa. **C:** Quantitative assessment of ^{22}Na uptake in MDCKI-hNCC cells grown on semi-permeable supports or plastic. Cells were grown until confluency prior to treatment +/- tetracycline for 16-20 hours. Subsequently, cells were incubated in uptake medium +/- metolazone. In cells grown on either semi-permeable supports or plastic, ^{22}Na uptake is increased following tetracycline induction. However, ^{22}Na uptake is significantly lower in cells grown on plastic compared to semi-permeable supports. Data are means ± S.E.M. (*n*=6) *Represents significant differences compared to MDCKI-hNCC cells grown on filters without metolazone inhibition. **Represents significant differences compared to MDCKI-hNCC cells grown on plastic without metolazone inhibition. **D:** Immunoblots of NCC expression in MDCKI-hNCC cells grown on semi-permeable supports or plastic. 20S proteasome abundance is a loading control. **E:** Semi-quantitative assessment of NCC levels in MDCKI-hNCC cells grown on semi-permeable supports compared to plastic. NCC abundance is significantly lower in cells grown on plastic supports. Data are means ± S.E.M. (*n*=3) *Represents significant difference compared to cells grown on filters.

Fig 4: Characterization of ^{22}Na uptakes in MDCKI-hNCC cells grown on plastic. A: Effect of incubation time on ^{22}Na uptake. Tetracycline induced cells were incubated in uptake medium +/- metolazone for 0 to 120 min. Data are means ± S.E.M. (*n*=4 per time point). There was time-linearity up to 40 min (r^2 = 0.95). **B:** Effect of metolazone on ^{22}Na

617 uptake. Uptakes were performed with the indicated metolazone concentrations and data
618 fitted to a non-linear curve with Graphpad Prism. Data are means ± S.E.M. (*n*=6). The
619 calculated IC50 of metolazone was 0.43 x 10^{-6} **C:** Chloride dependency of ^{22}Na uptake in
620 MDCKI-hNCC cells. Tetracycline induced cells were pre-incubated in chloride free (CF)
621 medium, before uptakes were performed +/- chloride or metolazone as indicated. ^{22}Na
622 uptake in MDCKI-hNCC cells is not significantly different from baseline uptake when chloride
623 is absent from uptake medium. Data are means ± S.E.M. (*n*=12) *Represents significant
624 differences compared to chloride-containing uptake medium without metolazone.
625
626 **Fig 5: Lowering chloride in the pre-incubation medium increases ^{22}Na uptake and**
627 **apical membrane abundance of total NCC and pT58-NCC in MDCKI-hNCC cells. A:**
628 Immunoblots showing effects of low chloride (LC) stimulation on total NCC abundance and
629 apical plasma membrane NCC and pT58-NCC abundance in MDCKI-hNCC cells grown on
630 plastic. 20S proteasome abundance in total homogenates is a loading control. B**:** Semi-
631 quantitative assessment of biotinylated NCC levels under control or LC conditions. Plasma
632 membrane NCC abundances significantly increase in MDCK-hNCC cells following LC pre-
633 incubation. Data are means ± S.E.M. (*n*=3) *Represents significant difference compared to
634 control. C**:** Semi-quantitative assessment of biotinylated pT58-NCC levels following pre-
635 incubation under control or LC. Plasma membrane pT58-NCC abundances are significantly
636 increased with LC pre-incubation. Data are means ± S.E.M. (*n*=3) *Represents significant
637 difference compared to control. **D:** Quantitative assessment of the effect of chloride-free
638 (CF) pre-incubation on ^{22}Na uptake. Tetracycline induced cells were pre-incubated with CF
639 or chloride–containing buffer for 20 min prior to incubation in uptake medium +/- metolazone.
640 ^{22}Na uptake is significantly greater when MDCKI-hNCC cells are pre-incubated in CF buffer.

641 Data are means ± S.E.M. (*n*=12) *Represents significant differences compared to CF pre-
642 incubation without metolazone. **Represents significant differences compared to chloride-
643 containing pre-incubation without metolazone.
644
645 **Fig 6: Acute changes in extracellular K^+ concentration modulates pT58-NCC levels in**
646 **MDCKI-hNCC cells. A:** Immunoblots of total NCC and pT58-NCC on total lysates from filter-
647 grown MDCKI-hNCC cells treated for 15 min in different extracellular [K^+]. Low chloride
648 buffer acts as a positive control. B**:** Semi-quantitative assessment of extracellular K^+
649 manipulation. Data are means ± S.E.M. (*n*=9) *Represents significant difference compared
650 to 3 mM conditions.
651
652 **Fig 7: Role of phosphorylation at Thr53, Thr58, and Ser71 in rNCC in MDCKI-rNCC**
653 **cells. A:** NCC immunoprecipitated from MDCKI-rNCC cells using a rabbit FLAG-tag
654 antibody. NCC is detected as a non-glycosylated band of approximately 100 kDa, a
655 glycosylated band around 130 kDa and a higher molecular weight protein above 250 kDa
656 (possible glycosylated NCC dimers). **B:** Representative immunoblots of MDCKI-rNCC cells
657 or MDCKI cells expressing phospho-deficient (TTS-AAA) or phospho-mimicking (TTS-DDD)
658 NCC mutants. **C:** qRT-PCR to determine mRNA expression of NCC in MDCKI-rNCC, TTS-
659 AAA, or TTS-DDD mutant cells. NCC mRNA levels are similar in the three different cell lines.
660 **D:** Metolazone-sensitive ^{22}Na uptakes in various MDCKI-rNCC cell lines. Tetracycline
661 induced cells were pre-incubated in chloride-free (CF) or chloride-containing (CC) medium
662 before incubation in uptake medium +/- metolazone as indicated. Metolazone-sensitive
663 uptake is the difference in ^{22}Na uptake between groups treated with and without metolazone.
664 Preventing phosphorylation of NCC at Thr53, Thr58, and Ser71 inhibits ^{22}Na uptake,

665 whereas mimicking phosphorylation on the same sites renders rNCC constitutively active.
666 Data are means ± S.E.M. (*n*=12) *Represents significant difference compared to MDCKI-
667 rNCC wt pre-incubated in CF medium.
668

669 **Table 1. Comparison of various systems for assessing NCC function**
670

System for studying NCC	Advantage	Disadvantage
Xenopus laevis oocyte	Easily obtained, large and hardy.	Relatively labor intensive with microinjection of each oocyte
	Few endogenous channels or transporters, resulting in low background transport	Non-native promoter and cannot be used to study NCC transcription (mRNA levels)
	Do not depend on extracellular resources for nutrition	Derived from poikilothermic animal and temperature-sensitive processes may be altered compared to mammalian cells.
	Good technical reproducibility	Accessory proteins may be different from mammalian cells
	Readily express NCC RNA that is transcribed to large amounts of exogenous protein	GPCRs and subsequent signaling cascades may be altered compared to mammalian cells
	Suitable for assessing the function of NCC mutants	Polarized NCC trafficking is not the same as mammalian cells
Transiently transfected cells (HEK, CHO)	Easy to transfect in high efficiency	Non-native promoter and cannot be used to study NCC transcription (mRNA levels)
	Suitable for assessing the function of NCC mutants	Not polarized and thus regulated delivery of NCC to the cell surface may be different from native cells
	Several of the GPCRs, signaling cascades and signaling specificities are comparable to native DCT cells	Suffer from differences in gene copy number and mRNA expression making comparisons between mutants difficult
Endogenous NCC-expressing cells	Native promoter and can be used to study NCC transcription (mRNA levels)	Unsuitable for assessing the function of NCC mutants
	Several GPCRs and subsequent signaling cascades are comparable to native DCT cells	Low NCC signal to noise
	Form polarized monolayer with apical membrane NCC expression	NCC exists predominantly as a high-mannose glycoprotein
Inducible NCC expressing MDCKI cells (current study)	Highly characterized mammalian cell system for studying regulated protein trafficking	Non-native promoter and cannot be used to study NCC transcription (mRNA levels)
	Form polarized monolayer with apical membrane NCC expression	Derived from dog, so commercially available reagents e.g. shRNA or antibodies against relevant NCC modulating proteins are difficult to obtain
	NCC is complex glycosylated and forms functional dimers	
	Several GPCRs and subsequent signaling cascades are comparable to native DCT cells	
	Suitable for assessing the function of NCC mutants	
	Single copy of NCC gene in cell genome making comparisons between mutants simple difficult	

671

672

673

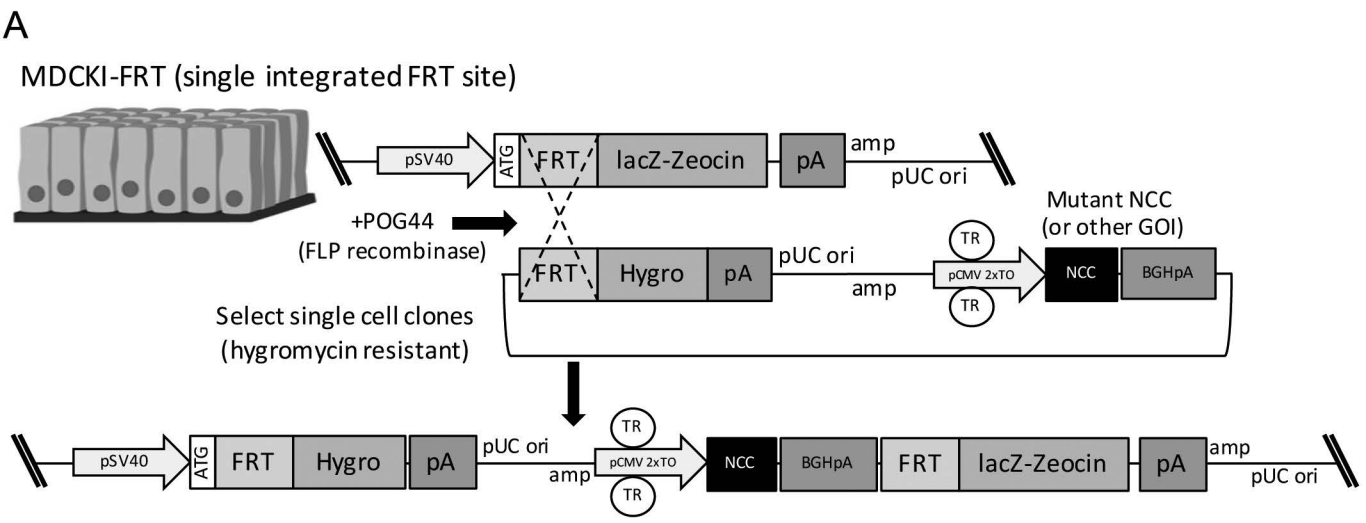
A
MDCKI-FRT (single integrated FRT site)
pSV40
ATG
FRT
lacZ-Zeocin
pA
amp
pUC ori
+POG44
(FLP recombinase)
Mutant NCC
(or other GOI)
FRT
Hygro
pA
pUC ori
amp
TR
pCMV 2xTO
TR
NCC
BGHpA
Select single cell clones
(hygromycin resistant)
pSV40
ATG
FRT
Hygro
pA
pUC ori
amp
TR
pCMV 2xTO
TR
NCC
BGHpA
FRT
lacZ-Zeocin
pA
amp
pUC ori
Single copy of NCC (or other GOI) stably intergrated into MDCKI cells and mRNA expression controlled by tetracyline

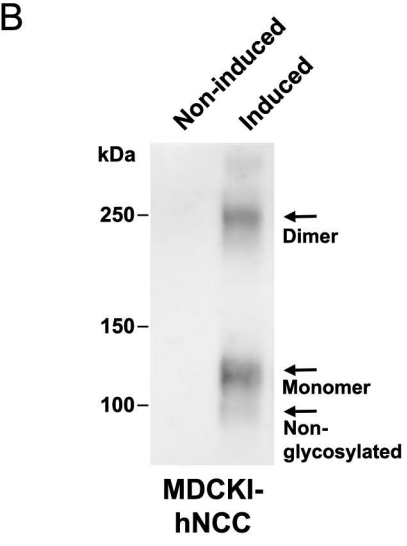
B
Non-induced
Induced
kDa
250
150
100
Dimer
Monomer
Non-
glycosylated
MDCKI-
hNCC

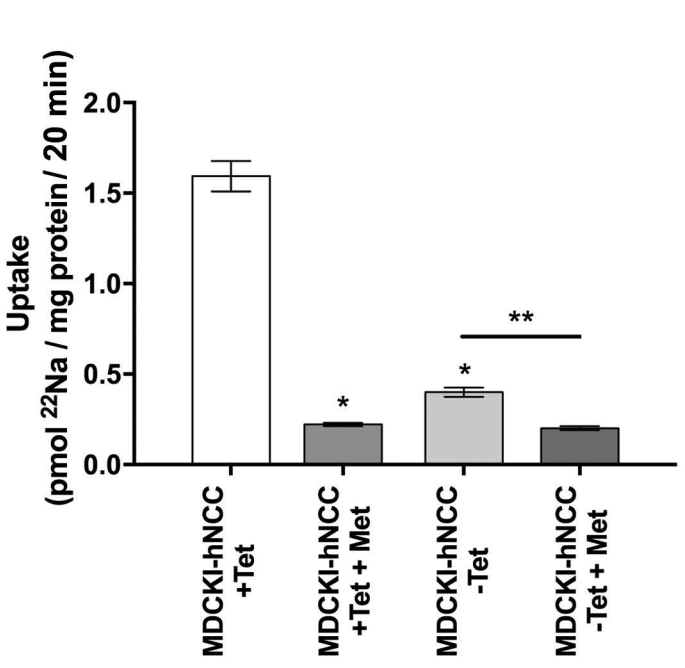
C
Uptake
(pmol 22Na / mg protein / 20 min)
2.0
1.5
1.0
0.5
0.0
*
*
**
MDCKI-hNCC
+Tet
MDCKI-hNCC
+Tet + Met
MDCKI-hNCC
-Tet
MDCKI-hNCC
-Tet + Met

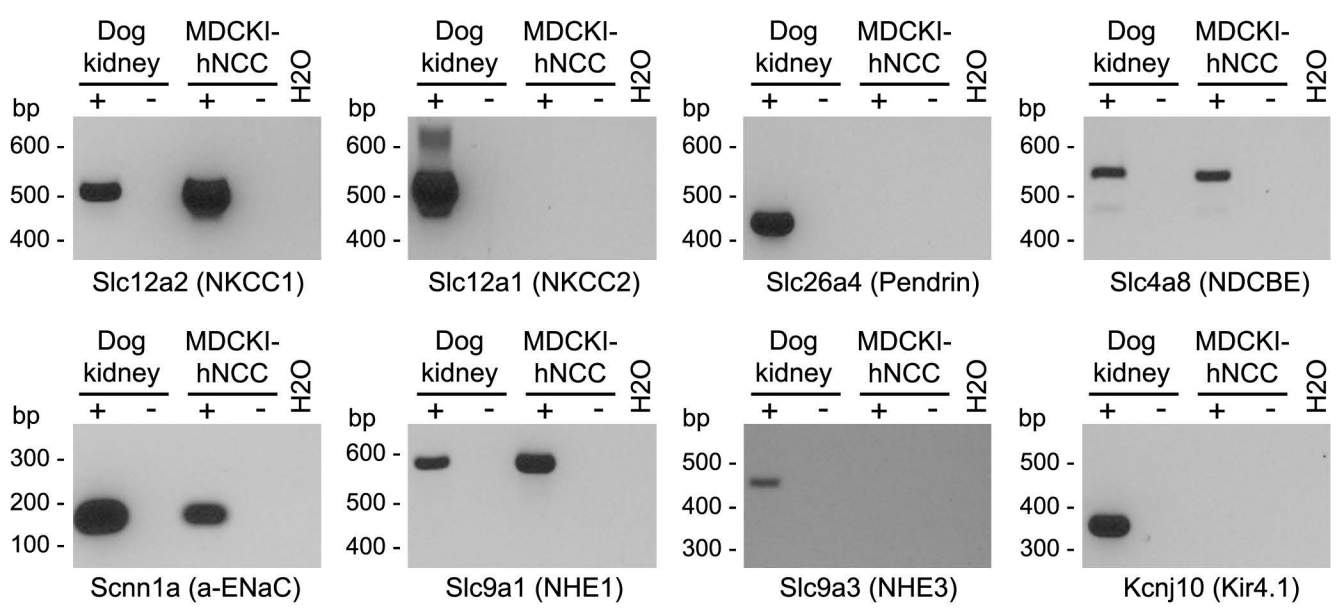
Dog kidney
MDCKI-hNCC
H2O
+ - + -
bp
600 -
500 -
400 -
Slc12a2 (NKCC1)
Slc12a1 (NKCC2)
Slc26a4 (Pendrin)
Slc4a8 (NDCBE)
300 -
200 -
100 -
Scnn1a (a-ENaC)
Slc9a1 (NHE1)
Slc9a3 (NHE3)
Kcnj10 (Kir4.1)

A

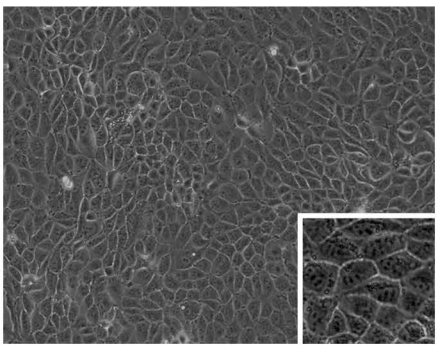

B

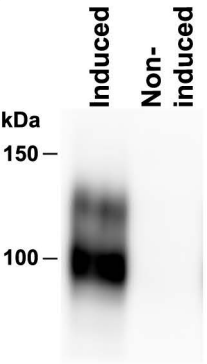
Induced
Non-induced
kDa
150
100

C

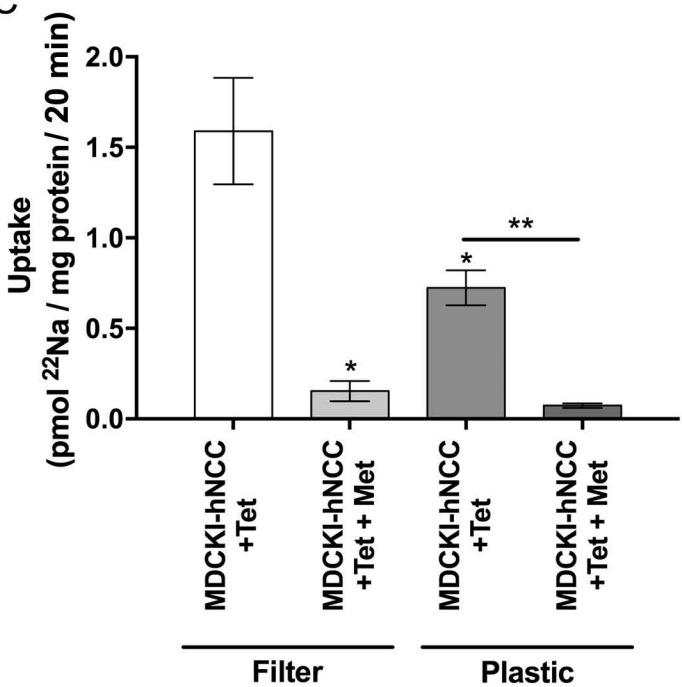
Uptake
(pmol 22Na / mg protein / 20 min)
2.0
1.5
1.0
0.5
0.0
*
*
**
MDCKI-hNCC +Tet
MDCKI-hNCC +Tet + Met
MDCKI-hNCC +Tet
MDCKI-hNCC +Tet + Met
Filter
Plastic

D

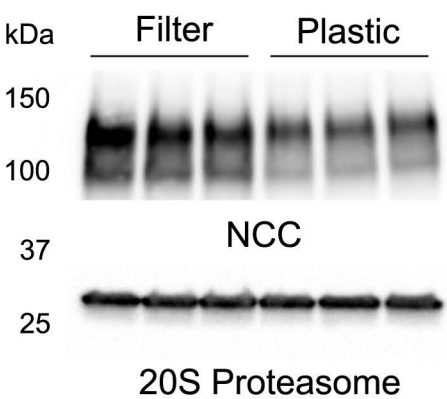
kDa
Filter
Plastic
150
100
NCC
37
25
20S Proteasome

E

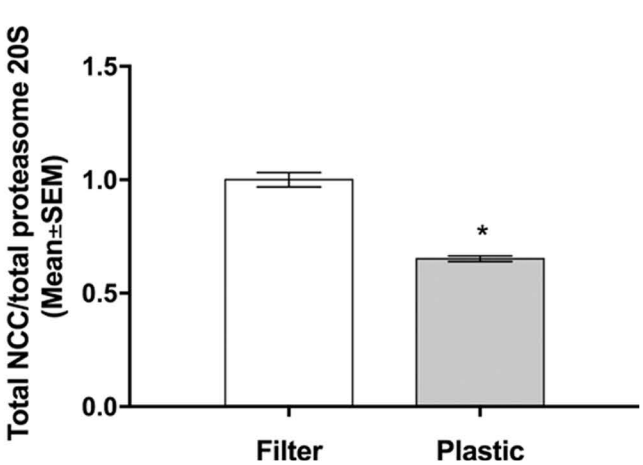
Total NCC/total proteasome 20S
(Mean±SEM)
1.5
1.0
0.5
0.0
*
Filter
Plastic

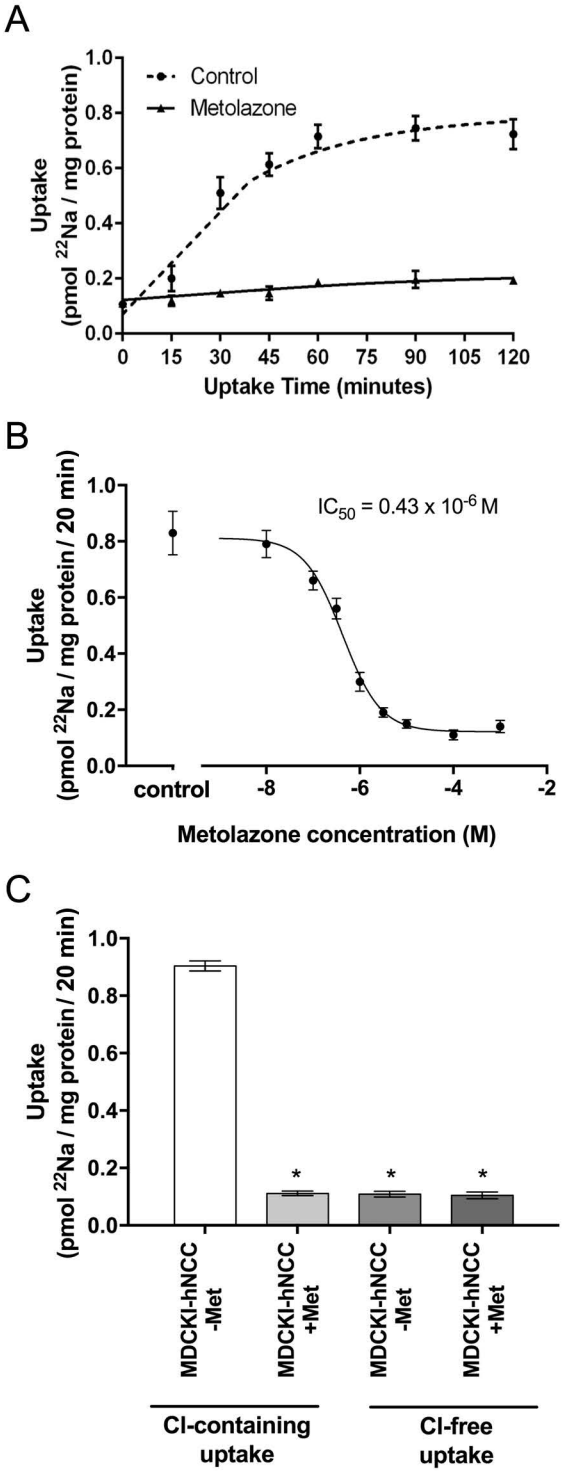
A
Control
Metolazone
Uptake
(pmol 22Na / mg protein)
1.0
0.8
0.6
0.4
0.2
0.0
0
15
30
45
60
75
90
105
120
Uptake Time (minutes)
B
Uptake
(pmol 22Na / mg protein / 20 min)
IC50 = 0.43 x 10-6 M
control
-8
-6
-4
-2
Metolazone concentration (M)
C
Uptake
(pmol 22Na / mg protein / 20 min)
MDCKI-hNCC -Met
MDCKI-hNCC +Met
MDCKI-hNCC -Met
MDCKI-hNCC +Met
Cl-containing uptake
Cl-free uptake

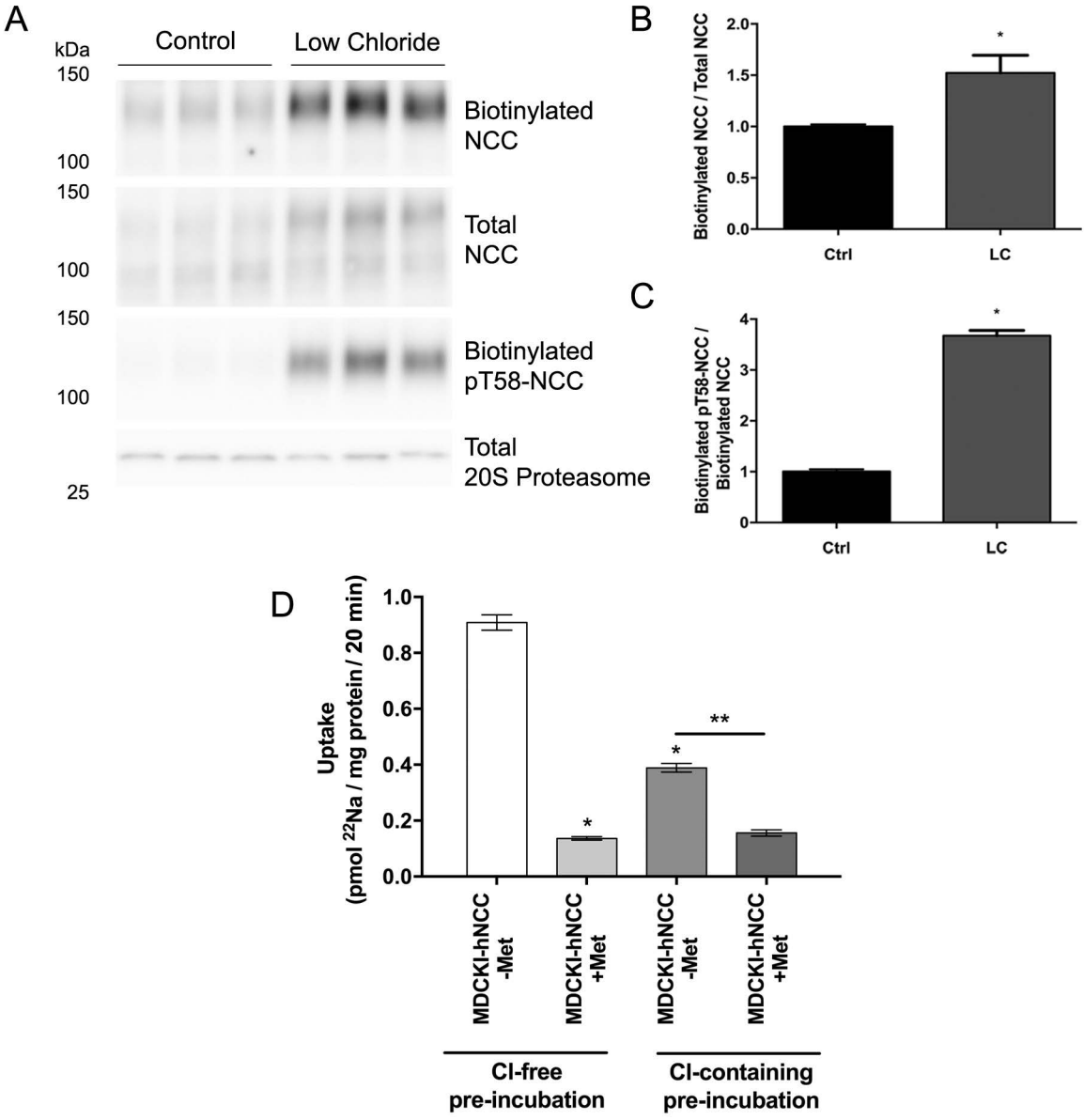
A
kDa
Control
Low Chloride
150
100
Biotinylated NCC
Total NCC
Biotinylated pT58-NCC
Total 20S Proteasome
25
B
Biotinylated NCC / Total NCC
Ctrl
LC
C
Biotinylated pT58-NCC / Biotinylated NCC
D
Uptake (pmol 22Na / mg protein / 20 min)
MDCKI-hNCC -Met
MDCKI-hNCC +Met
Cl-free pre-incubation
Cl-containing pre-incubation

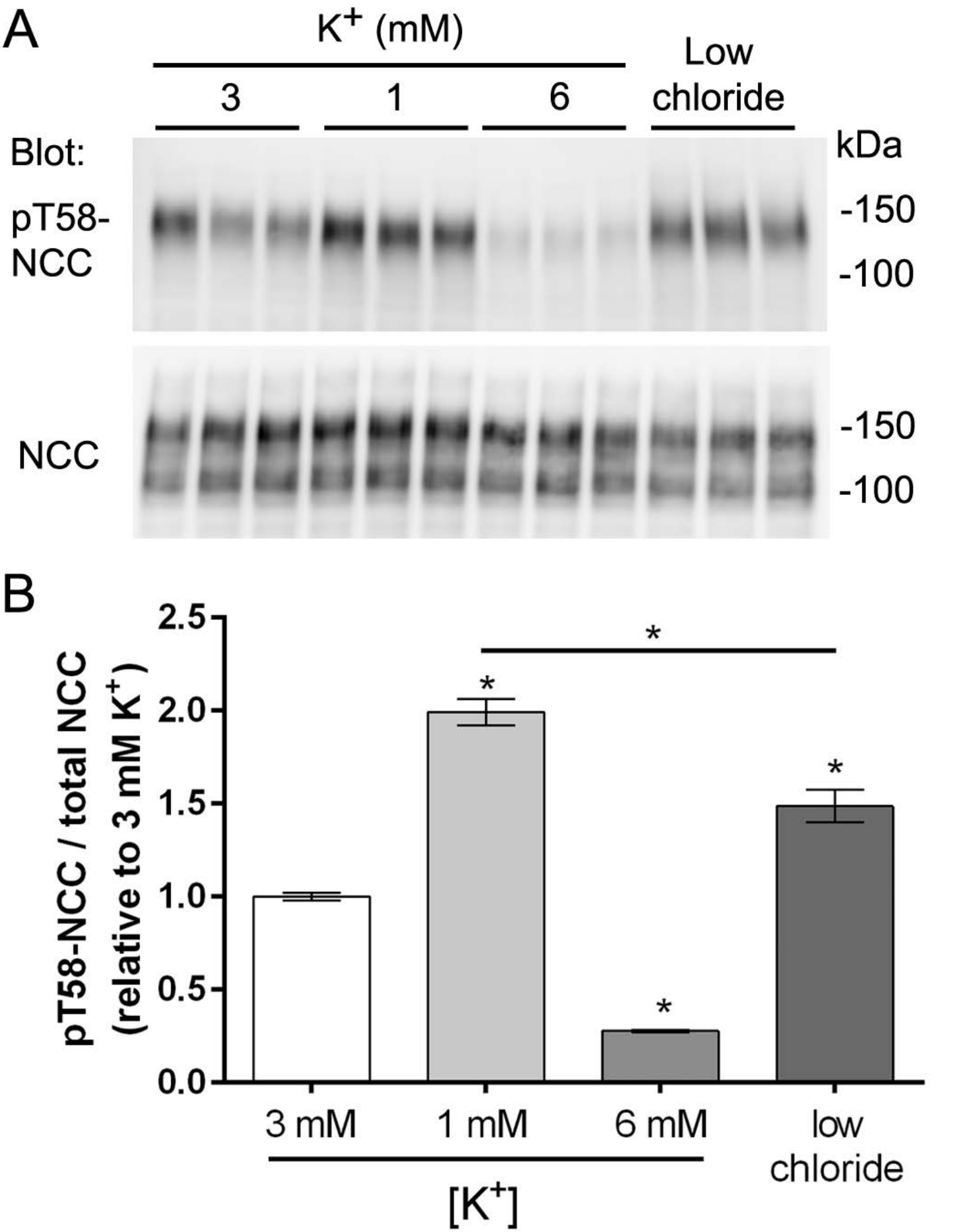
A
K+ (mM)
3
1
6
Low chloride
Blot:
pT58-NCC
NCC
kDa
-150
-100
-150
-100
B
pT58-NCC / total NCC (relative to 3 mM K+)
2.5
2.0
1.5
1.0
0.5
0.0
*
*
*
*
3 mM
1 mM
6 mM
low chloride
[K+]

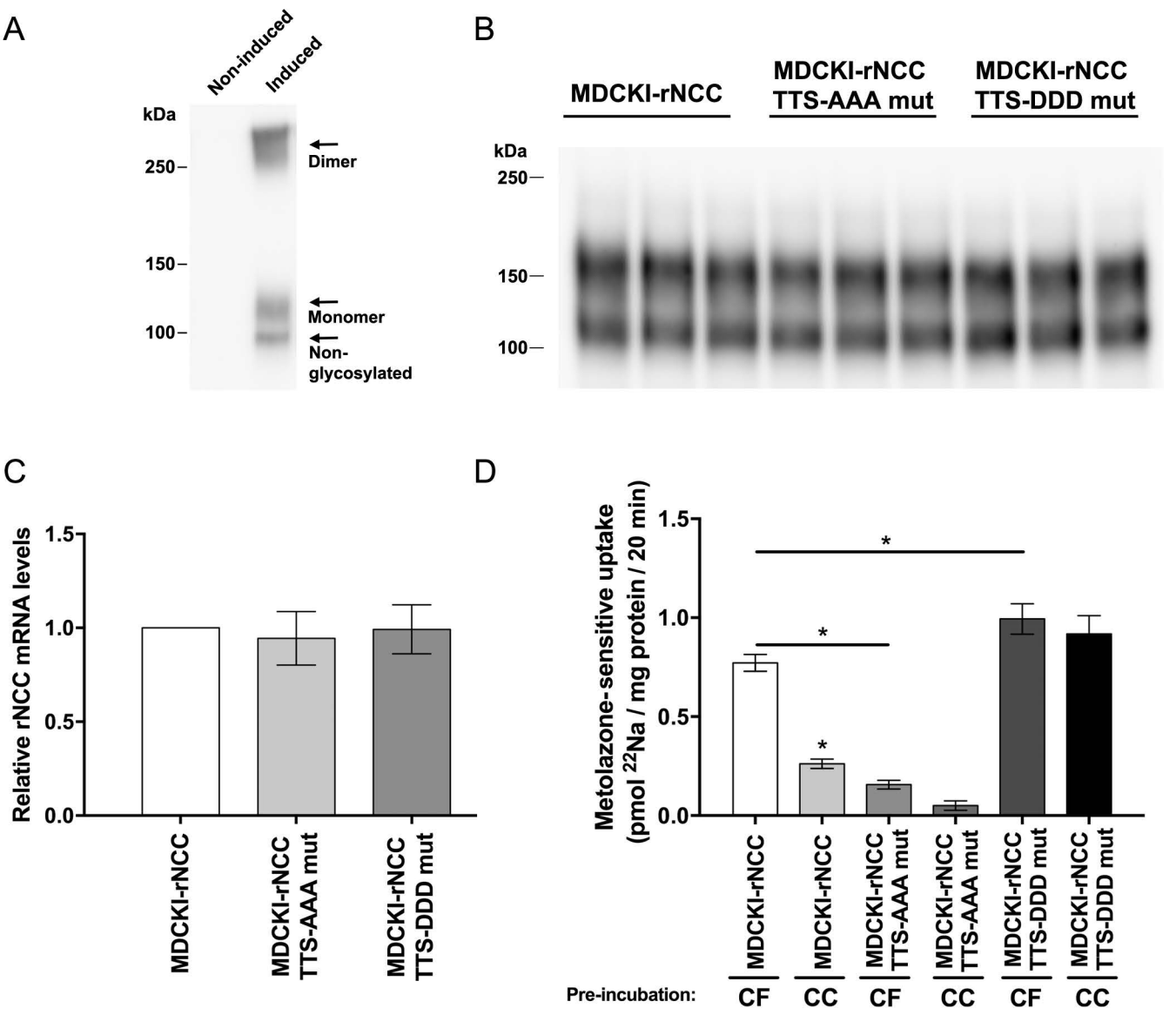
A
Non-induced
Induced
kDa
250
150
100
Dimer
Monomer
Non-glycosylated
B
MDCKI-rNCC
MDCKI-rNCC TTS-AAA mut
MDCKI-rNCC TTS-DDD mut
kDa
250
150
100
C
Relative rNCC mRNA levels
1.5
1.0
0.5
0.0
MDCKI-rNCC
MDCKI-rNCC TTS-AAA mut
MDCKI-rNCC TTS-DDD mut
D
Metolazone-sensitive uptake (pmol ^{22}Na / mg protein / 20 min)
1.5
1.0
0.5
0.0
*
*
*
MDCKI-rNCC
MDCKI-rNCC TTS-AAA mut
MDCKI-rNCC TTS-DDD mut
Pre-incubation:
CF
CC
CF
CC
CF
CC